

Two-stream instability analysis for propagating charged particle beams with a velocity tilt

D. V. Rose,* T. C. Genoni, and D. R. Welch
Voss Scientific, LLC, Albuquerque, New Mexico 87108, USA

E. A. Startsev and R. C. Davidson
Princeton Plasma Physics Laboratory, Princeton, New Jersey 08543, USA
 (Received 15 January 2007; published 28 March 2007)

The linear growth of the two-stream instability for a charged-particle beam that is longitudinally compressing as it propagates through a background plasma (due to an applied velocity tilt) is examined. Detailed, 1D particle-in-cell (PIC) simulations are carried out to examine the growth of the wave packet produced by a small amplitude density perturbation in the background plasma. Recent analytic and numerical work by Startsev and Davidson [Phys. Plasmas **13**, 062108 (2006)] predicted reduced linear growth rates, which are indeed observed in the PIC simulations. Here, small-signal asymptotic gain factors are determined in a semianalytic analysis and compared with the simulation results in the appropriate limits. Nonlinear effects in the PIC simulations, including wave breaking and particle trapping, are found to limit the linear growth phase of the instability for both compressing and noncompressing beams.

DOI: [10.1103/PhysRevSTAB.10.034203](https://doi.org/10.1103/PhysRevSTAB.10.034203)

PACS numbers: 52.35.Qz, 52.59.-f, 52.65.Rr

I. INTRODUCTION

Longitudinal drift compression of ion beams is being studied as a means to achieve short-duration, high-energy-density pulses for warm-dense-matter [1,2] and heavy ion inertial fusion energy [3–6] applications. Longitudinal compression is driven by a velocity profile or *tilt* on a charged-particle beam that is applied either at the source as part of the beam generation (as in some high power diodes) or by passing the beam through a programmed accelerating structure.

Recent experiments at Lawrence Berkeley National Laboratory have successfully demonstrated controlled longitudinal drift compression of heavy ion beams [7–10]. A velocity tilt was applied to an unneutralized, drifting ion beam using an induction core, and then the beam entered a plasma-filled drift region where longitudinal compression factors, J_{bF}/J_{b0} , over 60 were achieved, where J_{b0} and J_{bF} are the initial and peak compressed beam current densities, respectively. At the end of this drift region, radial compression of the beam will be attempted by passing the longitudinally compressing beam through a plasma-filled solenoid.

Theoretical modeling supporting both the design and analysis of these experiments has been carried out using analytic methods [11] and numerical simulations [12–16]. As this modeling is extended to parameter regimes beyond current experimental values to future higher-energy-density applications, careful consideration of the growth and saturation of a number of potential beam-plasma instabilities must be considered [17–23]. Recently, a detailed theoretical study of two-stream instability growth for a

longitudinally compressing charged-particle beam propagating in a background plasma was published [24]. An analytic asymptotic gain function for the instability was obtained and compared to numerical solutions of the original system of linearized equations. Reduced two-stream instability growth, relative to the case of a noncompressing beam, was found. This reduced growth is mainly attributable to the detuning of the primary unstable wave number as the beam propagates and compresses.

Here, we seek comparisons of theoretical estimates for the growth of the two-stream instability with particle-in-cell (PIC) simulations, a critical design and analysis tool for ion beam drift compression experiments and future higher-energy-density systems. The PIC model can also be used to examine instability saturation mechanisms and other nonlinear effects [25–27], which are difficult to assess from a purely analytic approach. In order to compare the two-stream instability model of Ref. [24] to our simulation results, we have derived a semianalytic asymptotic gain formula that is valid in the limit of small-signal growth at early times (and propagation distances) which is described in Sec. II. The PIC simulation model used here is described in Sec. III and results are presented in Sec. IV.

II. ANALYSIS

An electron beam of initial length $2L_{b0}$ is propagating in the x direction in a background plasma. The midpoint of the beam length, initially at position $x = X_0 = 0$ at time $t = 0$, moves at speed V_{b0} and has an initial uniform density n_{b0} . This beam speed increases linearly back from the point X_0 (and decreases linearly in the direction towards the beam head), allowing the beam to longitudinally compress as it propagates forward. The time of

*Electronic address: David.Rose@vosssci.com

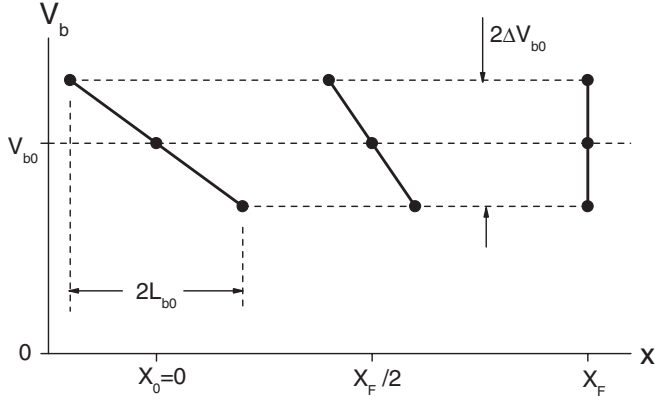


FIG. 1. Beam phase-space at 3 times in terms of the variables defined in the text.

(idealized) maximum compression is $t = T_F$, which occurs at position $x = X_F = T_F V_{b0}$. The longitudinal velocity is given by

$$V_b(x, t) = \frac{V_{b0} T_F - x}{T_F - t}, \quad (1)$$

and the velocity tilt is then defined as the ratio

$$\frac{\Delta V}{V_{b0}} = \frac{L_{b0}}{X_F}, \quad (2)$$

where ΔV is indicated schematically in Fig. 1, showing the idealized beam phase-space at 3 times in terms of the variables given here.

The beam density increases as the beam propagates forward as

$$n_b(t) = n_{b0} \frac{X_F}{X_F - V_{b0} t}, \quad (3)$$

where n_{b0} is the initial beam density. To ensure adequate charge and current neutralization, we assume $n_{b0}/n_{p0} \ll 1$, where n_{p0} is the initially uniform background plasma density. For the parameters used here, the beam density remains smaller than the plasma density over all but the final times of the propagation. This assumption does not include nonideal effects such as finite beam and plasma temperatures, which can further limit the small beam-to-plasma density ratio assumption. These effects are not included in this analysis, but can be examined in the PIC simulations.

A. Linearized small-signal equations

We use the linearized continuity and momentum equations for the plasma and beam electrons from Startsev and Davidson [24] coupled with Poisson's equation [see Eqs. (13) and (14) of Ref. [24]]. These equations represent the standard system of perturbed fluid equations typically used in the analysis of the two-stream instability [28], suitably modified to account for the longitudinal compression

of the beam (retaining relevant first-order terms for the beam density and velocity).

B. Asymptotic solution

Startsev and Davidson [24] obtained an approximate Laplace transform solution to the system of equations describing the perturbed electron beam density [see Eq. (35) of Ref. [24]]. They identified the phase associated with this perturbed beam electron density as [see Eq. (36) of Ref. [24]]

$$\phi(s) = -i\tau s \pm 2\alpha\sqrt{1-X}W, \quad (4)$$

where $X = x/X_F$, $s = \omega/\omega_{pe}$, $\tau = \omega_{pe}(t - x/V_{b0})$, ω_{pe} is the electron plasma frequency, and

$$W = \int_{\sqrt{1-X}}^1 \left[\left(\frac{1}{s} + z^2 \right) \left(\frac{1}{s} - z^2 \right) \right]^{-1/2} dz. \quad (5)$$

A saddle point analysis yielded the gain function

$$G(X) = \alpha\sqrt{2(1-X)}F[\arccos(\sqrt{1-X})], \quad (6)$$

where $\alpha = \omega_{be} T_F$, ω_{be} is the beam electron plasma frequency, and

$$F(x) = \int_0^x \left(1 - \frac{1}{2} \sin^2 \theta \right)^{-1/2} d\theta \quad (7)$$

is the elliptic integral of the first kind. This asymptotic solution (6) is only valid for $\tau \gg \alpha\sqrt{1-X}$, which is for positions (and times) far behind the beam head. Also we note that Eq. (6) is not valid in the limit $X \ll 1$.

For direct comparison with PIC simulations, we require an asymptotic solution that is valid at times and positions nearer the initial perturbation. In the limit that $s \simeq 1 + \epsilon$, $\epsilon \ll 1$, and $X \ll 1$, the integral W can be approximated as (see the Appendix)

$$W \simeq \frac{i}{\sqrt{2}} (\sqrt{\epsilon - X} - \sqrt{\epsilon}). \quad (8)$$

With this expression for W we look for saddle points of

$$\phi(\epsilon) = -i\tau(1 + \epsilon) - i\sqrt{2}\alpha\sqrt{1-X}(\sqrt{\epsilon - X} - \sqrt{\epsilon}). \quad (9)$$

Setting $\partial\phi/\partial\epsilon = 0$ gives

$$\frac{1}{\sqrt{\epsilon}} - \frac{1}{\sqrt{\epsilon - X}} = \frac{\sqrt{2}\tau}{\alpha\sqrt{1-X}}. \quad (10)$$

Solution of Eq. (10) for ϵ (for a given τ and X) and substitution back into Eq. (4) gives the asymptotic gain. Although solutions are easily obtained with readily available numerical packages, Eq. (10) can be rearranged to give a quartic equation in ϵ . We find that the fourth order term is generally small and can be ignored, resulting in the following cubic equation:

$$(2\bar{\tau}^4 X + 4\bar{\tau}^2)\epsilon^3 - (\bar{\tau}^4 X^2 + 6\bar{\tau}^2 X)\epsilon^2 + (2\bar{\tau}^2 X^2)\epsilon - X^2 = 0, \quad (11)$$

where

$$\bar{\tau} = \frac{\sqrt{2}\tau}{\alpha\sqrt{1-X}}.$$

The positive imaginary root of the cubic form can be identified and written out for comparison with the ‘‘no tilt’’ (NT) case. After some simplifications that take into consideration the limit $X \ll 1$, the root in question can be approximated as

$$\epsilon_T = f_1(u, X) - \frac{1}{2}\left(\frac{\alpha^2 X^2}{8\tau^2}\right)^{1/3} f_2^+(u, X) + i\frac{\sqrt{3}}{2}\left(\frac{\alpha^2 X^2}{8\tau^2}\right)^{1/3} f_2^-(u, X), \quad (12)$$

where

$$f_1(u, X) = \frac{X(6+u)}{6(2+u)},$$

$$f_2^\pm(u, X) = \frac{[g(1-X)]^{1/3}}{1+u/2} \left[1 \pm \left(\frac{u}{2g}\right)^{2/3} \frac{1+u^2/12}{3} \right],$$

$$g(u) \simeq 1 + u + \frac{u^2}{12} + \frac{u^4}{216},$$

and $u = \bar{\tau}^2 X$. This root can be compared directly with the equivalent root from the standard two-stream analysis (without a velocity tilt) [28] which can be written as

$$\epsilon_{\text{NT}} = -\frac{1}{2}\left(\frac{\alpha^2 X^2}{8\tau^2}\right)^{1/3} + i\frac{\sqrt{3}}{2}\left(\frac{\alpha^2 X^2}{8\tau^2}\right)^{1/3}. \quad (13)$$

In the limit $X_F \rightarrow \infty$, we observe $f_1(u, X) \rightarrow 0$, and $f_2^\pm(u, X) \rightarrow 1$, which gives $\epsilon_T = \epsilon_{\text{NT}}$, confirming that for increasingly smaller velocity tilts, the $\Delta V/V_{b0} = 0$ two-stream gain function is recovered.

III. PIC SIMULATION MODEL

The PIC code LSP [29] is used in 1D to examine the gain from the two-stream instability for charged-particle beams propagating in a background plasma with and without an applied velocity tilt. The simulations are electrostatic and use a cloud-in-cell model [30] to help minimize electrostatic fluctuations on the grid. This same simulation model has been used previously to examine a number of wave-particle and wave-wave interactions including 1D and 2D studies of streaming instabilities [21,22,31], Landau damping [32], and drift cyclotron instabilities [33].

A perturbation of the plasma electron density at $t = 0$ and $x = 0$ of the form

$$n_{pe} = \begin{cases} n^\dagger \exp(-a|x|), & \text{for } x > 0 \\ -n^\dagger \exp(-a|x|), & \text{for } x < 0 \end{cases} \quad (14)$$

is used, where n^\dagger is the density perturbation amplitude and the coefficient a determines the characteristic width of the perturbation. This provides an impulselike electric field that excites a growing wave packet.

The simulations use four separate charged-particle species to represent the (initially) charge and current-neutral beam-plasma system. Electrons and ions with equal velocity and number density (with $m_{bi} = 10^9 m_e$, where m_{bi} and m_e are the beam ion and electron masses) are initially propagating in a charge-neutral, cold-background electron-ion plasma ($m_{pi} = 10^9 m_e$, where m_{pi} is the plasma ion mass). The very high (essentially infinite) ion masses used in the simulations effectively eliminate ion-electron and ion-ion modes from the analysis.

For all cases, the simulations are initialized with 100 particles per cell (combined beam and plasma particles), $\Delta t = 3 \times 10^{-4}$ ns, and $\Delta x = 0.01$ cm, where Δt and Δx are the (constant) time step and cell size. Nominal two-stream wavelengths for our parameters are $\lambda = 2\pi V_{b0}/\omega_{pe} \simeq 0.33$ cm, which are well resolved by Δx as are plasma oscillations $\omega_{pe}\Delta t \simeq 0.017 < 1/2$. The simulation length $L = 150$ cm is much longer than the total propagation distances studied. The initial beam length $2L_{b0} = 55$ cm and the perturbation described in Eq. (14) is initialized at $x = 0$ cm, which for all cases is the center of the beam and this position corresponds to $v_b = V_{b0} = 0.1c$, where c is the speed of light. Periodic boundaries are used to eliminate space charge waves that are driven by typical sheath formation at conducting boundaries. Also, the sharp-edge density discontinuity at the beam head and tail creates space charge waves that can propagate into the beam. Consideration of these effects guided the selection of the parameters, balancing growth of the wave packet from the initial programmed perturbation against these nonideal disturbances.

A sample simulation result for the case with $\Delta V/V_{b0} = 0.2$ (vtilt10 in Table I) is illustrated in Figs. 2 and 3. The evolution of the beam electrons in time is traced in Fig. 2, which overlays the (x, v_x) phase-space of the beam electrons at 5 times (0, 2, 4, 6, and 8 ns). As the beam drifts forwards, the perturbation is growing and convecting at a speed slightly faster than the ‘‘classical’’ estimate of the

TABLE I. Summary of cold-plasma, cold-beam two-stream simulations. For all cases, $V_{b0} = 0.1c$, $n_p = 10^{12}$ cm $^{-3}$, $n_b = 10^8$ cm $^{-3}$, $a = 5$ cm $^{-1}$, and $L_{b0} = 27.5$ cm.

Run ID	$\Delta V/V_{b0}$	X_F (cm)	T_F (ns)
vtilt11	0	∞	∞
vtilt10	0.2	275.0	91.67
vtilt12	0.4	137.5	45.83
vtilt13	0.6	91.67	30.56

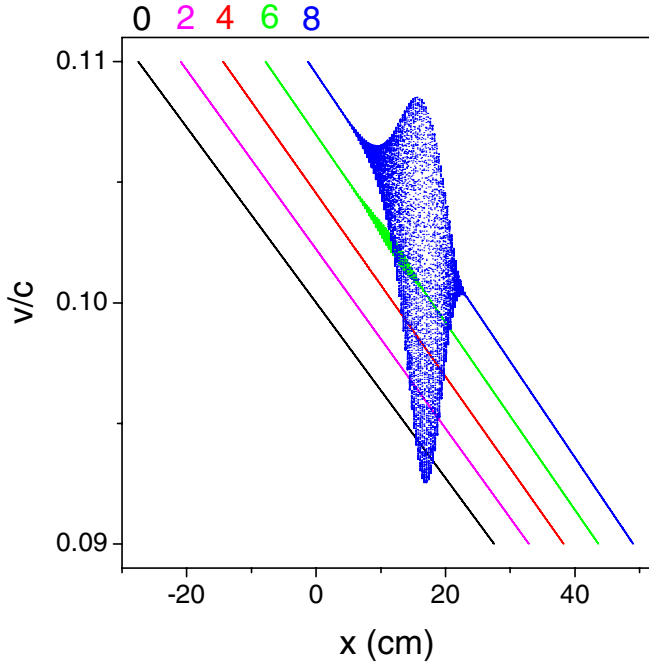


FIG. 2. (Color) Evolution of the beam electron (x, v_x) phase-space for a drifting beam with $\Delta V/V_{b0} = 0.2$ at 2-ns intervals (labeled at the top of the plot).

two-stream group velocity $v_g = 2V_{b0}/3$. On this scale, the electron response is only visible at $t \geq 6$ ns.

The total electric field energy associated with the evolution of this wave packet is tracked in the simulation by a diagnostic window that moves in the beam propagation

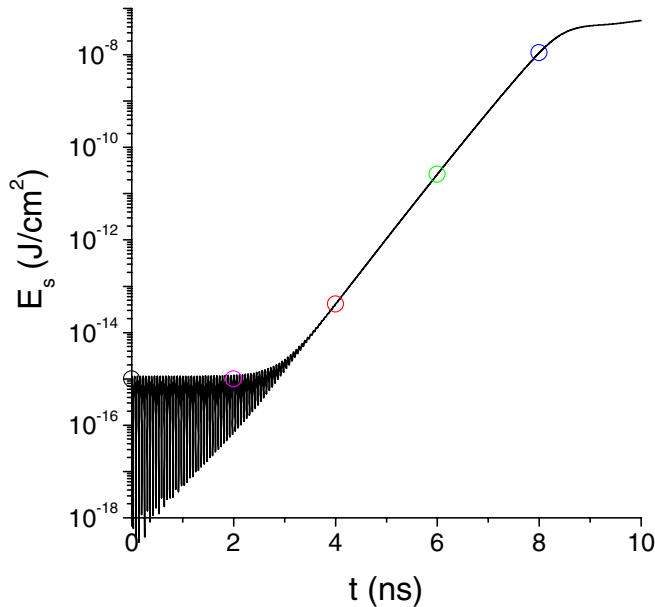


FIG. 3. (Color) Wave packet energy as a function of time for a 20-cm wide window moving at $2V_{b0}/3$. The individual points correspond to the electron beam phase-space times shown in Fig. 2.

direction at speed v_g . This electrostatic energy E_s is plotted for run vtilt10 in Fig. 3 as a function of time. The diagnostic window is 20-cm wide and initially centered around $x = 0$. The individual data points (open circles) correspond to the times of the phase-space plots in Fig. 2. The wave energy level rises linearly over approximately 6 orders of magnitude before leveling off at $\sim 3 \times 10^{-8}$ J/cm². Relative to the beam electron phase-space at 8 ns (Fig. 2), this transition represents the end of the linear growth phase and corresponds to the onset of nonlinear effects including wave breaking and particle trapping [25–27].

This nonlinear phase is illustrated in Fig. 4 which plots the electric field, beam electron phase-space and beam electron number density at $t = 9$ ns, which corresponds to the beginning of the plateau in electrostatic wave energy shown in Fig. 3. At this time, the electric field wave packet is beginning to distort (the onset of wave breaking), as shown in Fig. 4(a). (Note that this time and corresponding

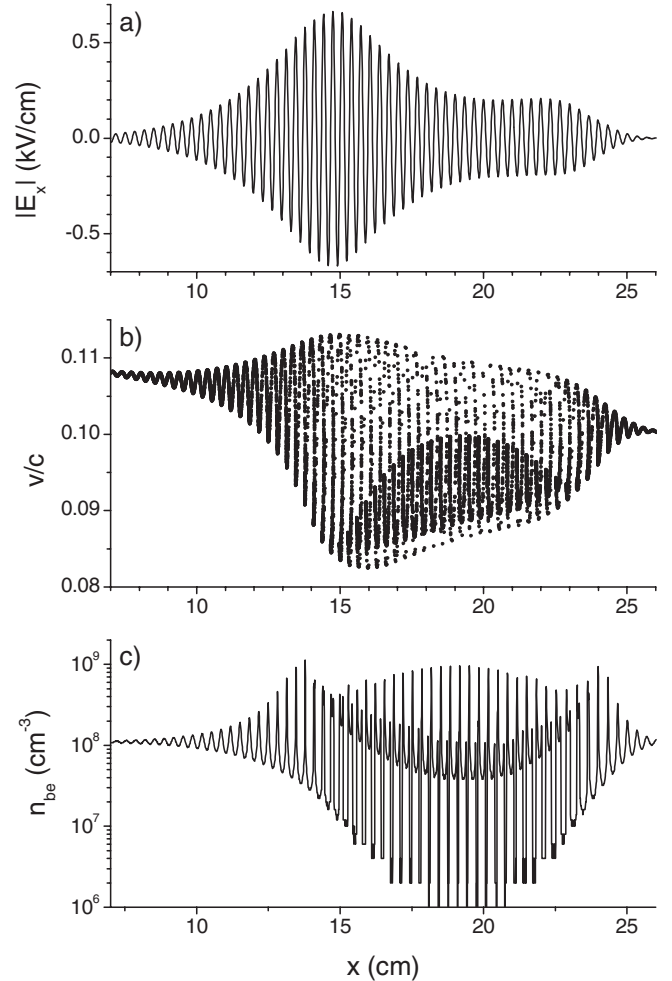


FIG. 4. Sample data taken from the initial nonlinear phase of the simulation, $t = 9$ ns. The electric field wave packet is shown in (a), the beam electron phase-space in (b), and the beam electron density in (c).

propagation distance is much smaller than T_F and X_F for this case as given in Table I.) A lobe on the electron phase-space volume has folded back into the main body at small values of v/c , as shown in 4(b), illustrating the onset of particle trapping. This fold initially acts to fill in the beam density between the small wavelength oscillations, as shown in 4(c), which, in turn, acts to partially damp the electric field oscillations. Within another 3 ns (about 170 plasma periods), the beam electrons begin to thermalize within the wave packet.

IV. SIMULATION RESULTS AND MODEL COMPARISON

A series of four PIC simulations with different velocity tilts ($\Delta V/V_{b0}$) are presented and compared with the model developed in Sec. II. The simulations are listed in order of increasing $\Delta V/V_{b0}$ in Table I. For all cases $V_{b0} = 0.1c$, $n_{pe} = n_{pi} = 10^{12} \text{ cm}^{-3}$, $n_{be} = n_{bi} = 10^8 \text{ cm}^{-3}$, $a = 5 \text{ cm}^{-1}$, $n^\dagger = 10^6 \text{ cm}^{-3}$, $L = 150 \text{ cm}$, and $L_{b0} = 55 \text{ cm}$. The first simulation listed in Table I uses a constant velocity beam (no tilt), which corresponds to infinite values of X_F and T_F .

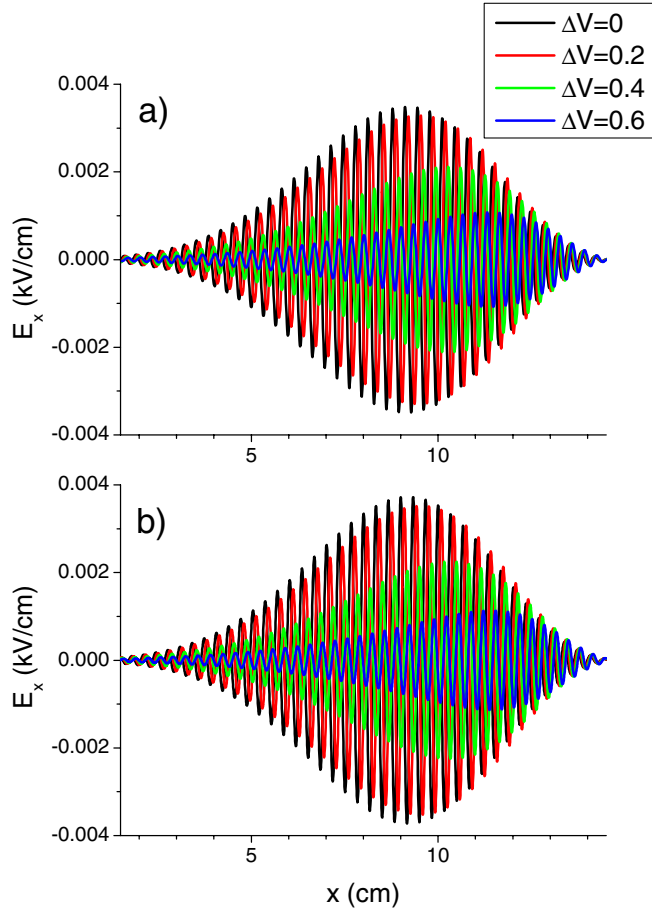


FIG. 5. (Color) Comparison of electric field wave packets with different velocity tilts at $t = 5 \text{ ns}$ from (a) the PIC simulations and (b) numerical solution of the perturbed fluid equation.

The relative growth of the electric field wave packet as a function of the beam velocity tilt is illustrated in Fig. 5 at $t = 5 \text{ ns}$ for all four velocity tilt cases. The PIC simulation results are given in Fig. 5(a). A larger tilt results in smaller relative growth in the peak electric field and an increasing group velocity. For all cases, 5 ns is well before nonlinear saturation effects occur, as illustrated in Fig. 4. Numerical solutions of the perturbed fluid equations described in Sec. II A are shown in Fig. 5(b) for the same parameters. The overall agreement in both the phase and amplitude of the wave packets for all velocity tilts confirms that the PIC simulations are still in the linear regime at $t = 5 \text{ ns}$.

The magnitude of the longitudinal electric field from the PIC simulations as a function of time 10 cm from the initial perturbation is shown in Fig. 6. This result further illustrates the slower unstable growth as a function of beam velocity tilt that is observed in Fig. 5.

The peak electric field as a function of time for these four simulations is plotted in Fig. 7. The asymptotic small-signal gain factor for the linear growth rate without a velocity tilt is [28]

$$G_{\text{NT}}(x, t) \approx \frac{3\sqrt{3}}{4} (k_{be}x)^{2/3} (\tau)^{1/3}, \quad (15)$$

and this equation is plotted in Fig. 7 as a black line. Here $k_{be} = \omega_{be}/V_{b0}$ and Eq. (15) is valid for $\tau \gg k_{be}x$. The remaining curves shown in Fig. 7 are determined by numerically maximizing Eq. (4) as a function of time for each velocity tilt. For comparison of the simulations with the asymptotic gain curves, we normalized the computed fields to $E_0 \approx 1.22 \times 10^{-6} \text{ kV/cm}$. This value brings the simu-

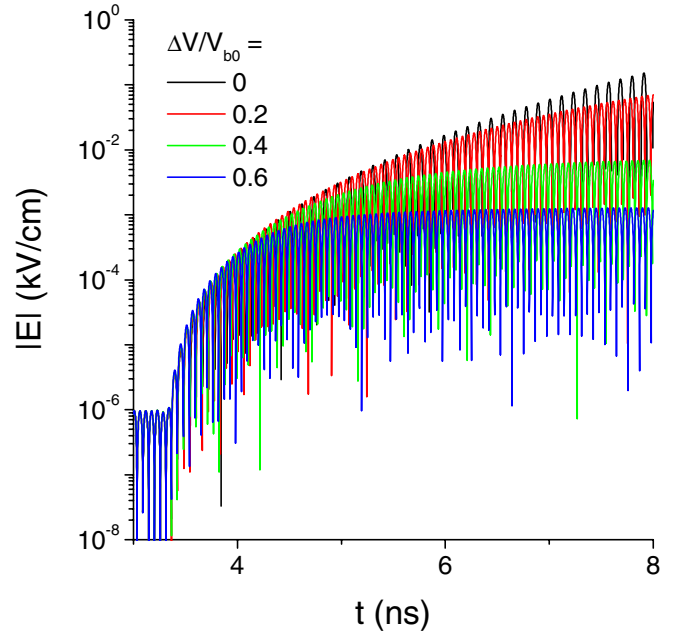


FIG. 6. (Color) Comparison of electric field magnitudes in the PIC simulations as a function of time at a point 10 cm downstream from the initial perturbation location.

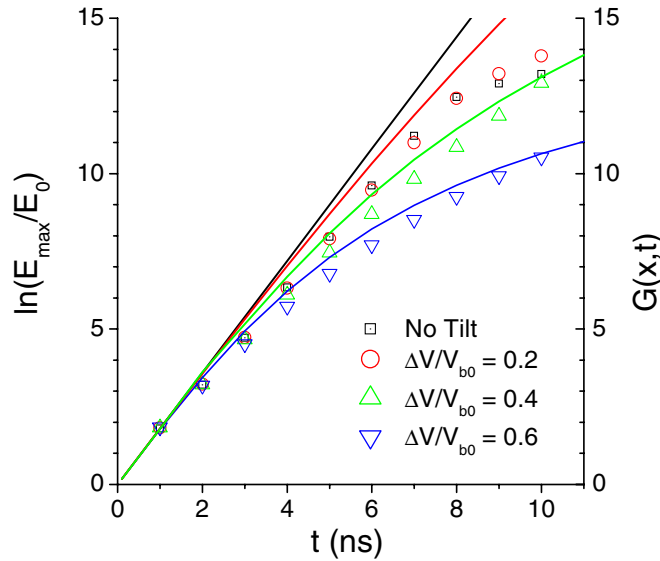


FIG. 7. (Color) The peak electric field signal amplitude E_{\max} as a function of time from the simulations (individual data points). The gain factor G_{NT} from Eq. (15) is plotted as a black line and the remaining lines are determined numerically from the solution of Eqs. (4) and (10).

lation gain for all four velocity tilts into agreement with the model gain at the earliest time ($t = 1$ ns). At later times, and hence larger gains, reduced instability growth due to increasing velocity tilt values is clearly observed, and the simulation results show trends that agree well with the asymptotic solutions. The agreement improves with increasing velocity tilt since the net gain is smaller and the validity of the approximations carried out as part of the analytic analysis then holds for longer times.

V. DISCUSSION AND CONCLUSIONS

A small-signal, early-time gain analysis has been carried out based on a system of model equations developed by Startsev and Davidson [24] to examine the linear growth of the two-stream instability for a longitudinally compressing charged-particle beam immersed in a background plasma. Here, we have extended the analysis of Ref. [24] to provide asymptotic gain estimates in the linear regime at small propagation distances and early times. The overall conclusion of Ref. [24] is that the two-stream growth rate is reduced for longitudinally compressing charged-particle beams. Our model results and PIC simulations support this conclusion. We note that the asymptotic analysis presented here correctly reduces to the well-established small-signal two-stream analysis for noncompressing beam [28].

One-dimensional PIC simulations have been carried out that support the conclusions of the model in the linear phase. In addition, these simulations can follow the non-linear evolution of the instability well beyond the limits of the asymptotic analysis. As noted above, a velocity tilt applied to charged-particle beams for longitudinal drift

compression does indeed result in a reduced growth rate for the longitudinal two-stream modes. However, technological constraints limit the velocity tilt that can be applied, at least for present applications [7–10]. Therefore, even these reduced growth rates are still significant. Careful evaluation of the nonlinear effects and possible coupling to emittance growth in charged-particle beams are important issues that need to be addressed as part of future accelerator designs supporting warm-dense-matter and heavy-ion-driven inertial fusion energy research.

ACKNOWLEDGMENTS

Funding was provided by the U.S. Department of Energy through the Princeton Plasma Physics Laboratory and the Heavy Ion Fusion Virtual National Laboratory.

APPENDIX

The evaluation of the integral W given in Eq. (5) from Sec. II is carried out in the limits $X \ll 1$ and $\epsilon \ll 1$. From standard integral tables [34], Eq. (5) is

$$W = \sqrt{\frac{s}{2}} [F(\gamma_2) - F(\gamma_1)], \quad (\text{A1})$$

with F given by Eq. (7) and

$$\gamma_1 = \arcsin\left(\frac{\sqrt{2s}\sqrt{1-X}}{\sqrt{s+1-sX}}\right),$$

$$\gamma_2 = \arcsin\left(\frac{\sqrt{2s}}{\sqrt{s+1}}\right).$$

For $s \approx 1 + \epsilon$ and $\gamma_i \approx \pi/2 - \delta_i$,

$$\sin\gamma_1 \approx 1 - \frac{\delta_1^2}{2} \approx \frac{\sqrt{(1+\epsilon)(1-X)}}{\sqrt{1+\epsilon/2-X/2}} \approx 1 + \frac{\epsilon-X}{4},$$

$$\sin\gamma_2 \approx 1 - \frac{\delta_2^2}{2} \approx \frac{\sqrt{1+\epsilon}}{\sqrt{1+\epsilon/2}} \approx 1 + \frac{\epsilon}{4},$$

which gives $\delta_1 \approx i\sqrt{(\epsilon-X)/2}$ and $\delta_2 \approx i\sqrt{\epsilon/2}$. Taylor expansion of F near γ_1 and γ_2 gives

$$F(\gamma_i) \approx F(\pi/2) + \left.\frac{\partial F}{\partial \gamma}\right|_{\pi/2} (-\delta_i), \quad (\text{A2})$$

with

$$\left.\frac{\partial F}{\partial \gamma}\right|_{\pi/2} = \sqrt{2}.$$

Substitution of Eq. (A2) into Eq. (A1) gives Eq. (8) for the integral W .

[1] N. A. Tahir *et al.*, Contrib. Plasma Phys. **43**, 373 (2003).

- [2] D. H. H. Hoffmann *et al.*, Phys. Scr. T **T123**, 1 (2006).
- [3] R. Goldston *et al.*, J. Fusion Energy **21**, 61 (2002).
- [4] J. D. Lindl, B. A. Hammel, B. G. Logan, D. D. Meyerhofer, S. A. Payne, and J. D. Sethian, Plasma Phys. Controlled Fusion **45**, A217 (2003).
- [5] B. G. Logan *et al.*, Nucl. Fusion **45**, 131 (2005).
- [6] M. M. Basko, Nucl. Fusion **45**, S38 (2005).
- [7] E. Henestroza *et al.*, Phys. Rev. ST Accel. Beams **7**, 083501 (2004).
- [8] P. K. Roy *et al.*, Nucl. Instrum. Methods Phys. Res., Sect. A **544**, 225 (2005).
- [9] P. K. Roy *et al.*, Phys. Plasmas **11**, 2890 (2004).
- [10] P. K. Roy *et al.*, Phys. Rev. Lett. **95**, 234801 (2005).
- [11] E. A. Startsev and R. C. Davidson, New J. Phys. **6**, 141 (2004).
- [12] H. Qin, R. C. Davidson, J. J. Barnard, and E. P. Lee, Phys. Rev. ST Accel. Beams **7**, 104201 (2004).
- [13] D. R. Welch, D. V. Rose, T. C. Genoni, S. S. Yu, and J. J. Barnard, Nucl. Instrum. Methods Phys. Res., Sect. A **544**, 236 (2005).
- [14] C. Thoma, D. R. Welch, S. S. Yu, E. Henestroza, P. K. Roy, S. Eylon, and E. P. Gilson, Phys. Plasmas **12**, 043102 (2005).
- [15] A. B. Sefkow and R. C. Davidson, Phys. Rev. ST Accel. Beams **9**, 090101 (2006).
- [16] D. R. Welch, D. V. Rose, C. Thoma, A. B. Sefkow, I. D. Kaganovich, P. A. Seidl, S. S. Yu, J. J. Barnard, and P. K. Roy (to be published).
- [17] R. C. Davidson, I. Kaganovich, H. Qin, E. A. Startsev, D. R. Welch, D. V. Rose, and H. S. Uhm, Phys. Rev. ST Accel. Beams **7**, 114801 (2004).
- [18] E. A. Startsev and R. C. Davidson, Phys. Rev. ST Accel. Beams **6**, 084401 (2003).
- [19] T. Kikuchi, M. Nakajima, K. Horioka, and T. Katayama, Phys. Rev. ST Accel. Beams **7**, 034201 (2004).
- [20] S. M. Lund and B. Bukh, Phys. Rev. ST Accel. Beams **7**, 024801 (2004).
- [21] T. C. Genoni, D. V. Rose, D. R. Welch, and E. P. Lee, Phys. Plasmas **11**, L73 (2004).
- [22] D. V. Rose, T. C. Genoni, D. R. Welch, and E. P. Lee, Nucl. Instrum. Methods Phys. Res., Sect. A **544**, 389 (2005).
- [23] R. C. Davidson, I. D. Kaganovich, E. A. Startsev, H. Qin, M. Dorf, A. B. Sefkow, D. R. Welch, D. V. Rose, and S. M. Lund (to be published).
- [24] E. A. Startsev and R. C. Davidson, Phys. Plasmas **13**, 062108 (2006).
- [25] N. A. Krall and A. W. Trivelpiece, *Principles of Plasma Physics* (San Francisco Press, New York, 1986).
- [26] R. C. Davidson, *Methods in Nonlinear Plasma Theory* (Academic Press, New York, 1972).
- [27] R. Z. Sagdeev and A. A. Galeev, *Nonlinear Plasma Theory* (W. A. Benjamin Press, New York, 1969).
- [28] R. J. Briggs, in *Advances in Plasma Physics*, edited by A. Simon and W. B. Thompson (Wiley Interscience, New York, 1971), Vol. 4, p. 43.
- [29] LSP is a software product of ATK Mission Research, Albuquerque, NM 87110.
- [30] C. K. Birdsall and A. B. Langdon, *Plasma Physics via Computer Simulation* (Adam Hilger, New York, 1991).
- [31] D. V. Rose, J. U. Guillory, and J. H. Beall, Phys. Plasmas **9**, 1000 (2002).
- [32] D. V. Rose, J. U. Guillory, and J. H. Beall, Phys. Plasmas **12**, 014501 (2005).
- [33] D. V. Rose, T. C. Genoni, D. R. Welch, T. A. Mehlhorn, J. L. Porter, and T. Ditmire, Phys. Plasmas **13**, 092507 (2006).
- [34] I. S. Gradshteyn and I. M. Ryzhik, *Table of Integrals, Series, and Products, Fourth Edition* (Academic Press, New York, 1980).